Element- and Time-Resolved Measurements of Spin Dynamics Using X-ray Detected Ferromagnetic Resonance

Christoph Klewe,[1] Qian Li,[2] Mengmeng Yang,[2] Alpha T. N'Diaye,[1]
David M. Burn,[3] Thorsten Hesjedal,[4] Adriana I. Figueroa,[3,5] Chanyong Hwang,[6]
Jia Li,[7] Robert J. Hicken,[8] Padraic Shafer,[1] Elke Arenholz,[9] Gerrit van der Laan,[3]
and Ziqiang Qiu[2]

[1]Advanced Light Source, Lawrence Berkeley National Laboratory, Berkeley, California, USA

[2]Department of Physics, University of California at Berkeley, Berkeley, California, USA

[3]Magnetic Spectroscopy Group, Diamond Light Source, Didcot, UK

[4]Department of Physics, Clarendon Laboratory, University of Oxford, Oxford, UK

[5]Catalan Institute of Nanoscience and Nanotechnology (ICN2), CSIC, Barcelona, Spain

[6]Korea Research Institute of Standards and Science, Yuseong, Daejeon, Republic of Korea

[7]International Center for Quantum Materials, School of Physics, Peking University, Beijing, China

[8]Department of Physics and Astronomy, University of Exeter, Exeter, Devon, UK

[9]Cornell High Energy Synchrotron Source, Cornell University, Ithaca, New York, USA

Introduction and overview

As existing CMOS-based nanoelectronics meets fundamental barriers, spintronic devices employing the electron spin in addition to or instead of the electron charge are being developed as an important new approach to continue miniaturization and scaling. In particular, the generation, manipulation, and detection of pure spin currents or spin-polarized charge currents are a key area of fundamental research. Advances in this area strongly rely on the development and optimization of more efficient detection methods. Ferromagnetic resonance (FMR) is a powerful tool for the study of magnetization dynamics. By using microwaves to excite the magnetization into a steady state of precession, insight may be gained into magnetic properties, such as magnetic damping and magnetic anisotropies in ferromagnetic materials, and even spin-orbit torque effects [1].

Recently, it has been shown that combining FMR with the capabilities of synchrotron radiation enables more detailed investigations of magnetization and spin dynamics [2–34]. The novel technique of X-ray detected FMR (XFMR) makes it possible to study the magnetization dynamics in an element-specific manner. The chemical and magnetic contrast in XFMR originates from X-ray magnetic circular dichroism (XMCD), an effect that has many disparate applications (see [33]). Time-resolved XFMR can be used to measure the amplitude and phase of the spin precession of each layer in a heterostructure system. However, such experiments pose a challenge because the precession frequency for ferromagnets is of the order of GHz and the precession cone angle is <1°. This problem can be solved by performing stroboscopic measurements

that utilize the time structure of the synchrotron (500 MHz), where the radio frequency (RF) magnetic field that drives the spin precession is synchronized with the X-ray pulses. Each X-ray pulse probes the magnetization cone at exactly the same point in the precession cycle. Thus, XFMR combines FMR and XMCD as follows: The sample is pumped by an RF magnetic field to generate a precession of the magnetization (i.e., FMR), which is then probed using the XMCD effect. Among other things, it turns out that XFMR has unique capabilities to probe spin-transfer torque (STT) [34, 35] and spin currents [34].

Experimentally, XFMR experiments can be divided into two distinct categories: time-averaged and time-resolved methods. Time-averaged measurements are typically carried out in a longitudinal geometry, where the magnetization M is oriented along the incident X-ray beam. In this configuration, the precession of the magnetic moments is excited at the ferromagnetic resonance and the change in the time averaged longitudinal component of the magnetization is recorded via resonant X-ray absorption. Since the collected signal is independent of the phase of precession of the magnetic moments, this method can be used at all excitation frequencies. In general, the time-averaged approach can provide information on the amplitude, resonance field, and linewidth of the ferromagnetic resonance with element, site, and valence state specificity, yet it does not provide any details about the phase of the magnetic precession.

Time-resolved measurements are performed in a transverse geometry, where the magnetization is oriented perpendicular to the incident X-ray pulses. In this geometry, the magnetic moments are continuously

excited by the RF field while the response from the phase-dependent magnetization components along the X-ray beam is probed stroboscopically. This pump-probe technique requires the microwave excitation to be synchronized to integer multiples of the X-ray pulse frequency and is typically limited to frequencies in the low GHz regime, due to the finite pulse length of the X-ray bunches.

The first XFMR experiments were carried out by Bailey et al. at Beamline 4-ID-C of the Advanced Photon Source (APS) in 2004 [2]. Using dynamic XMCD measurements, they demonstrated element-specific measurements of the magnetization precession of ferromagnetic $Ni_{81}Fe_{19}$, observing the Ni and Fe precession individually. Shortly after, Boero et al. [3] and Goulon et al. [4] performed similar XFMR measurements at the European Synchrotron Radiation Facility (ESRF), and Puzic et al. [5] demonstrated the first spatially resolved imaging of ferromagnetic eigenmodes at the Advanced Light Source (ALS). However, all of these pioneering works were carried out in the time-averaged measurement mode and did not yet provide information about the phase of the precession. The first layer- and time-resolved measurement of ferromagnetic resonance (FMR) in a $Ni_{81}Fe_{19}/Cu/Co_{93}Zr_7$ trilayer structure was demonstrated by Arena et al. [6] at the National Synchrotron Light Source, Brookhaven National Laboratory, in 2006. Their work first showed the possibility to detect both magnitude and phase information in the XFMR measurement.

Although XFMR experiments have been carried out at a number of synchrotron radiation facilities since 2004, only a few facilities currently have XFMR setups available for user operation. In this review, we mainly focus on recent developments and work that has been carried out using time-resolved XFMR at beamline 4.0.2 of the Advanced Light Source and at beamline I10 of the Diamond Light Source. The experimental setup and the sample holder used at beamline I10 and beamline 4.0.2, respectively, are shown in Figure 1. We will first introduce the working principle of XFMR and then provide examples of the capabilities of this technique. Finally, we will briefly describe an outlook for the future development of and new opportunities for XFMR.

Working principle of XFMR

A schematic illustration of the XFMR technique is shown in Figure 2. We distinguish between two different means of detecting the dynamic signal. The X-ray absorption is detected either as fluorescence yield (FY) from the direct excitation of photons from the absorbing material, or in a transmission geometry, as luminescence yield (LY) from a substrate subjacent to the film. In the LY configuration (see Figure 2(a)), the sample is mounted on a coplanar waveguide (CPW) with the film side facing the microwave resonator. A tapered hole in the center conductor (Figure 1(c, d)) allows the X-rays to penetrate the waveguide and hit the sample, while a photodiode mounted directly behind it collects
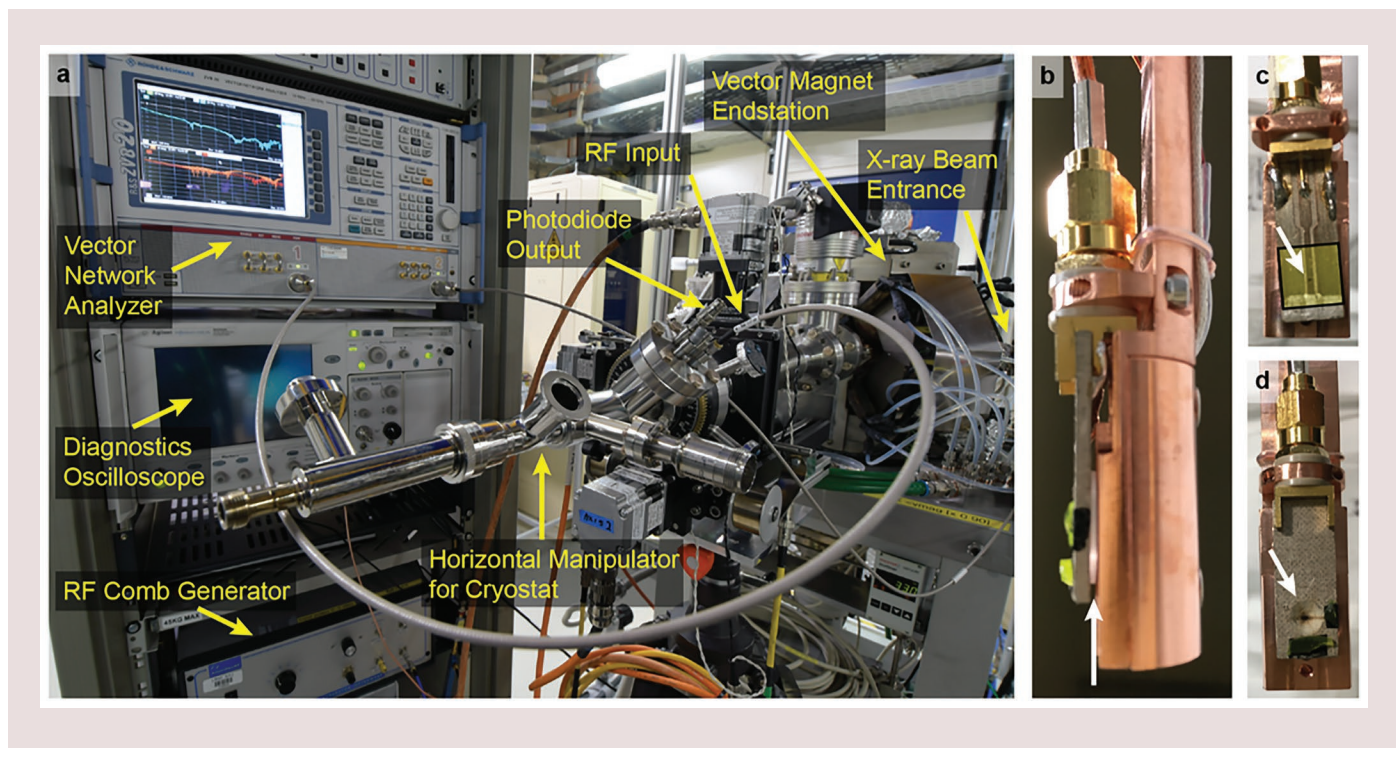

Figure 1: (a) Experimental setup at beamline I10 of the Diamond Light Source. (b–d) Luminescence yield sample holder used at beamline 4.0.2 of the Advanced Light Source. (b) The sample (arrow) is clamped between the CPW circuit board and the copper holder. The photodiode is encapsulated in the copper holder. (c) Front view of the sample on the CPW and (d) backside of the CPW circuit board with a tapered hole.
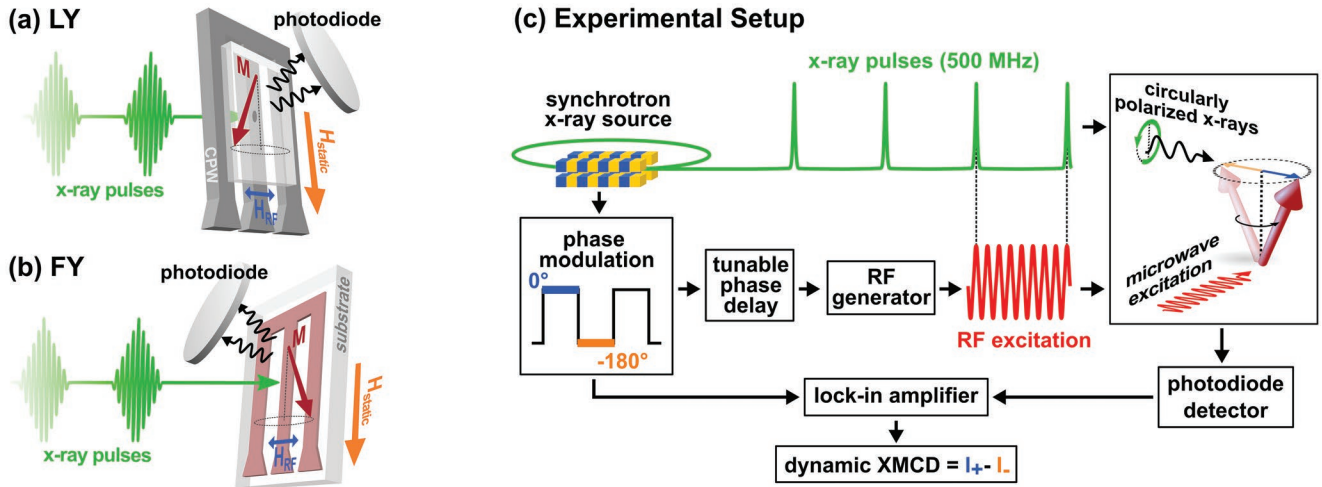
Figure 2: (a) Schematic illustration of the luminescence yield (LY) detection geometry. An unpatterned sample is mounted onto a coplanar waveguide with the film side facing the microwave resonator. The X-ray pulses propagate through a tapered hole in the center conductor to the film and the luminescence yield from the subjacent substrate is detected by a photodiode. (b) Schematic illustration of the fluorescence yield (FY) detection geometry. The X-ray beam is focused on a waveguide patterned into the sample and the fluorescence yield is detected by a photodiode. (c) Experimental setup of the XFMR measurements. Microwaves are generated at a frequency that is a higher harmonic of the 500 MHz storage ring frequency to ensure a fixed phase relationship between the RF pump field and the probing X-ray pulses. The phase of the RF excitation is modulated by 180° to probe the change in magnetization between opposite sides of the cone of precession.

the LY of the subjacent substrate. In the FY geometry (Figure 2(b)), the sample stack is patterned directly into a CPW geometry. The X-rays are focused on the center conductor and the FY from the film is detected by a photodiode mounted in front of the sample. The LY detection method enables the investigation of epitaxial thin films directly grown on a luminescent substrate (e.g., MgO, Al_2O_3, $MgAl_2O_4$, etc.) without the need for sample patterning, whereas the FY geometry allows for measuring lateral heterogeneity, though might require the films to be deposited on an additional conducting layer (e.g., Cu, Ag).

In both geometries, the XFMR is measured at fixed photon helicity with the film magnetization usually oriented along the CPW. An RF current provided to the CPW generates an RF magnetic field H_{RF} within the sample layer, leading to resonant excitation of the magnetization. As with conventional (i.e., static) XMCD spectroscopy, XFMR is sensitive to magnetization components along the incident beam. Thus, the RF-induced magnetization components of the precessional motion orthogonal to the static field can be detected with the incident beam perpendicular to the CPW.

In order to ensure a fixed phase relationship between the RF pump and the probing X-ray pulses, as required for a stroboscopic measurement, the frequency of the RF field must be a higher harmonic of the ~500 MHz synchrotron master oscillator frequency, and hence the electron bunches. Typically, the excitation frequency ranges from 1 GHz up to 5 GHz (12 GHz). Excitation frequencies exceeding this upper frequency show a strong suppression of the XFMR signal, due to the

blurring effect of the finite X-ray pulse length of 70 ps (34 ps) at the Advanced Light Source (Diamond Light Source).

To isolate the magnetic contrast, the phase of the RF excitation is modulated by 180° at a low frequency (e.g., between 100–1000 Hz) and the photodiode signal is fed into a lock-in amplifier (LIA). The LIA output corresponds to $I_{XFMR} = I_+ - I_-$ and probes the difference in X-ray absorption on opposite sides of the precession cone. By incrementally delaying the phase of the RF field with respect to the timing of the X-ray pulses, the complete precession cycle can be mapped, revealing detailed information about the amplitude and phase of the magnetic excitation. An example is shown in Figure 3.

Figure 3(a) displays a paradigm structure for the generation and detection of spin currents, consisting of a source layer, a combination of spacer and interlayers, and a sink layer. By exciting the source layer into ferromagnetic resonance, a spin current can be generated, as in conventional spin pumping experiments. The spin current then propagates through the spacer into the sink layer, where the response to the spin current is probed. Simultaneous excitation of the separate layers can be excluded by engineering the component layers to exhibit different resonance fields H_{ref}. By including different chemical elements within the different layers, and tuning of the photon energy to the corresponding element-specific XMCD peaks, which can be identified from static spectra, the spin dynamics of each layer may be investigated separately.

Results from XFMR measurements on a Py ($Ni_{80}Fe_{20}$) film, corresponding to the source layer in such a device, are shown in Fig-
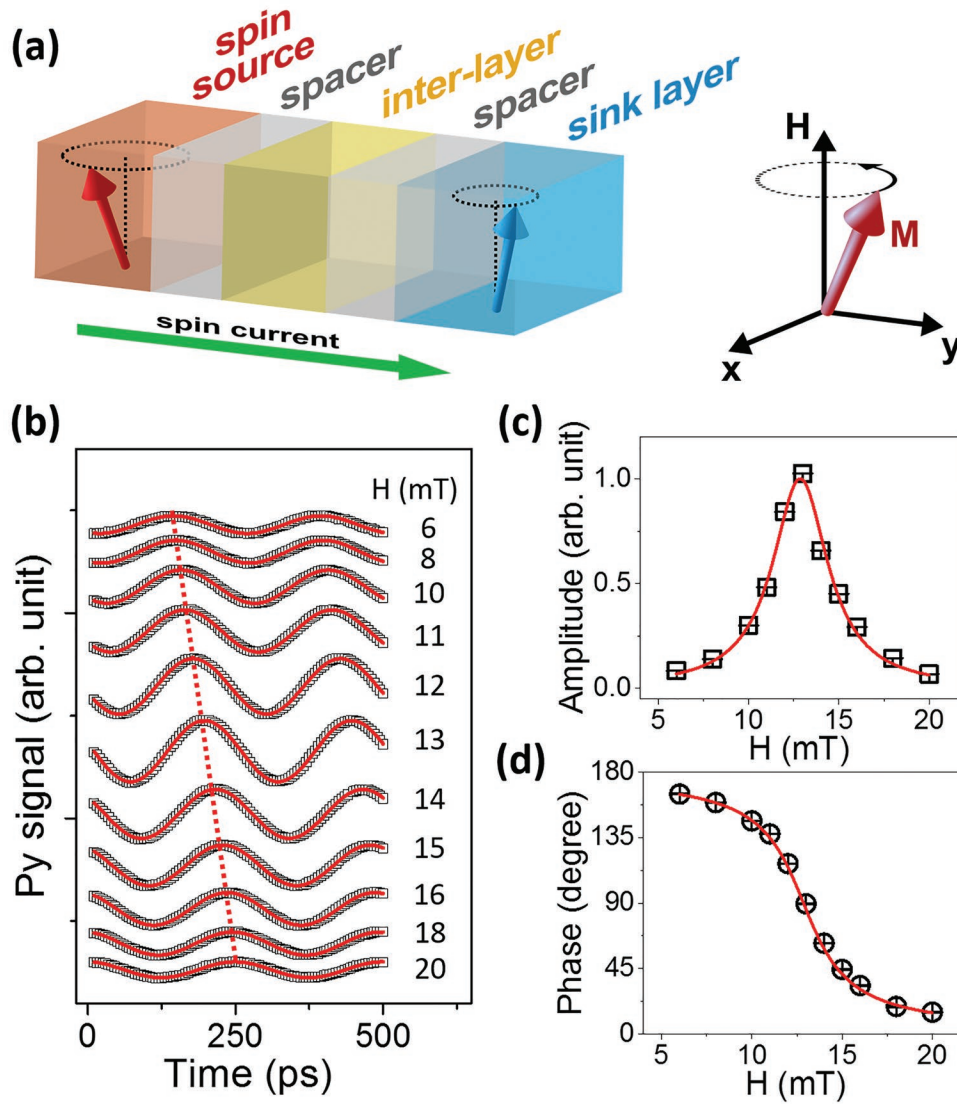
Figure 3: (a) Typical device architecture to generate and detect spin currents. (b) Phase delay scans at different bias fields across the ferromagnetic resonance of a Py film. (c) Amplitude and (d) phase, extracted from the phase delay scans.

ure 3(b). Phase delay scans were taken at the Fe L_3 edge (photon energy $\approx 707.8\,\text{eV}$) for different field values across the ferromagnetic resonance. Each of the scans was taken at a fixed bias field between 6 and 20 mT. The phase delay scans exhibit pronounced oscillations with a periodicity of 250 ps corresponding to the 4 GHz excitation frequency. The sinusoidal shape reflects the oscillatory motion of the precession. In order to rule out electrical pickup or other artificial effects as the origin of the observed oscillations, experiments may be made with opposite circular polarization to confirm that the sign of the signal is reversed.

By fitting a 4 GHz sine function to the curves, both the amplitude (Figure 3(c)) and the phase (Figure 3(d)) of the precession for each field value can be extracted. The amplitude of the absorption exhibits a Lorentzian shape, as expected for Gilbert-like damping. From the amplitudes, I_{XFMR} and I_{XMCD}, of the dynamic and the static XMCD, respectively, the cone angle θ can be determined via $\sin(\theta/2) = I_{\text{XFMR}}/I_{\text{XMCD}}$.

The phase exhibits a sigmoidal shape with a 180° shift across the resonance. The field dependence of the phase can be fitted with an arctan function. This behavior is characteristic of damped harmonic motion and indicates direct excitation by the RF field within the source

layer. The response from additional layers in the heterostructure can be investigated analogously, by measuring at the corresponding element-specific photon energies.

Element- and phase-resolved measurements

Exploiting the full potential of XFMR allows studying layer-specific magnetization precession in multilayers containing different elements. In particular, the investigation of spin current propagation through dif-ferent spacer layers can show intriguing effects and provide access to interesting physics. While the spin source and the sink layer displayed in the sample structure in Figure 3(a) typically consist of ferromagnetic materials, the interlayer material can vary— e.g., normal metal [26], topological insulator [21], antiferromagnetic (AFM) insulator [28], etc.—to study the effects on spin transport. Spacer layers with a high spin current transparency are inserted between the spin source (sink layer) and the interlayer to eliminate magnetic proximity effects [37] and reduce interlayer coupling [38].

Recently, a number of studies have investigated spin current transmission through antiferromagnetic insulators using electrical transport experiments. While these studies showed evidence for large DC spin current propagation through the AFM, with a strong enhancement around the antiferromagnetic Néel temperature, a detailed explanation for the mechanism behind these effects has remained outstanding.

In particular, these results raise the intriguing question of whether a GHz AC spin current remains coherent while propagating through an AFM insulator governed by THz AFM magnons. In order to study this fundamental question, Q. Li et al. [28] designed an epitaxial system of $Py/Ag/CoO/Ag/Fe_{75}Co_{25}$ (Figure 4(a)). Probing the spin precession in the spin source (Py) and the layer receiving the spin current ($Fe_{75}Co_{25}$) individually, by tuning the photon energy to the Ni and the Co absorption edges, respectively, enabled a detailed understanding of how a spin current is transmitted through the AFM insulator CoO. If the spacer layer thickness between the CoO interlayer and the sink layer is small, the spin precession in the $Fe_{75}Co_{25}$ layer is driven by a combination of the RF field, the effective $Py/Fe_{75}Co_{25}$ interlayer cou-pling, and the AC spin current generated by the Py excitation (Figure 4(b)). However, the phase resolution of XFMR allows the different contributions to the $Fe_{75}Co_{25}$ excitation to be distinguished. Specifically, the contributions from the RF field and the interlayer coupling to the spin source manifest as a sigmoidal phase behavior, whereas spin-current-induced excitation manifests as a bipolar phase shift across the resonance [25].

The effective magnetic interlayer coupling between the Py and $Fe_{75}Co_{25}$ magnetizations was designed to be switched on and off by tuning the thickness of the Ag spacer between the CoO and $Fe_{75}Co_{25}$. As the field is swept through the resonance of Py, the multilayer sample with a 2-nm-thick Ag spacer layer between the CoO and $Fe_{75}Co_{25}$ shows the characteristic sigmoidal phase shift of $Fe_{75}Co_{25}$ spin precession dominated by the effective $Py/Fe_{75}Co_{25}$ interlayer coupling. In contrast, the multilayer sample with 10-nm-thick Ag spacer layer

exhibits a bipolar phase shift of the $Fe_{75}Co_{25}$ spin precession—a fingerprint of spin-current-driven excitation (Figure 4(c)).

Using XFMR, Baker et al. [25] showed that spin pumping can display a pronounced angular dependence, arising from the relative alignment of the two magnetic layers and the magnitude of precession. The antiparallel alignment leads to more efficient absorption of the spin current as compensation of the pumped angular momentum is reduced. Similarly, damping is higher when the magnetization precession is out-of-phase. The XFMR studies on a $Co_{50}Fe_{50}/Cr/Ni_{81}Fe_{19}$ spin valve (Figure 4(d)) demonstrated that a strong anisotropy of spin pumping from the source layer can be induced by an angular dependence of the total Gilbert damping parameter α in the spin sink layer. Figures 4(e) and 4(f) show the phase of the $Co_{50}Fe_{50}$ spin precession across the $Ni_{81}Fe_{19}$ resonance for the field along the $Co_{50}Fe_{50}$ easy and hard axes of magnetization, respectively. Dashed lines correspond to the contribution of static coupling (interlayer) and dynamic coupling (spin current induced) decomposed from the field-dependent phase of the $Co_{50}Fe_{50}$ layer. The dynamic coupling (spin current) contribution was proven to be greater for the field along the $Co_{50}Fe_{50}$ hard axis than for the field along the easy axis. The in-plane variation of damping in the crystalline $Co_{50}Fe_{50}$ layer leads to an anisotropic α in the polycrystalline $Ni_{81}Fe_{19}$ layer. This anisotropy is suppressed above the spin diffusion length of Cr, which was found to be 8 nm, and which was independent of static exchange coupling in the spin valve. These results shed new light on the increasingly important topic of the anisotropic generation and detection of spin currents. They suggest the possibility of a further control of spin pumping through magnetization alignment, while also indicating new concepts to manipulate spin pumping through modification of the damping mechanisms in the spin sink layer.

Sensitivity of XFMR

XFMR has proven to be a highly sensitive technique, capable of probing small-angle precession within ultrathin layers of material. Multiple studies have shown that XFMR can not only measure the dynamics of ferromagnetic layers, but can also be used to probe spin currents in nonmagnetic layers [26] or detect excitations of uncompensated spins at the interface of an AFM insulator [28].

J. Li et al. [26] were able to trace a spin excitation from the spin source to the sink layer through a paramagnetic $Cu_{75}Mn_{25}$ spacer layer. As sketched in Figure 5(a), a spin current generated in the Py spin source induces a net spin precession in the $Cu_{75}Mn_{25}$ layer, even in the absence of a net magnetic moment. A measurement of the Mn spin precession using XFMR at the Py FMR field is shown in Figure 5(b). The result represents a direct detection of the pure AC spin current in the paramagnetic $Cu_{75}Mn_{25}$. From the Mn AC XMCD, the magnitude of the Mn moment due to the spin current can be estimated to be 2.5×10^{-3} μ_B/Mn, corresponding to a 6.5×10^{-5} μ_B DC Mn moment induced by the spin current.

It is well known that either oxygen migration at the interface to a metal layer or the magnetic proximity to a FM across a NM spacer layer can result in a small amount of uncompensated ferromagnetic Co spins
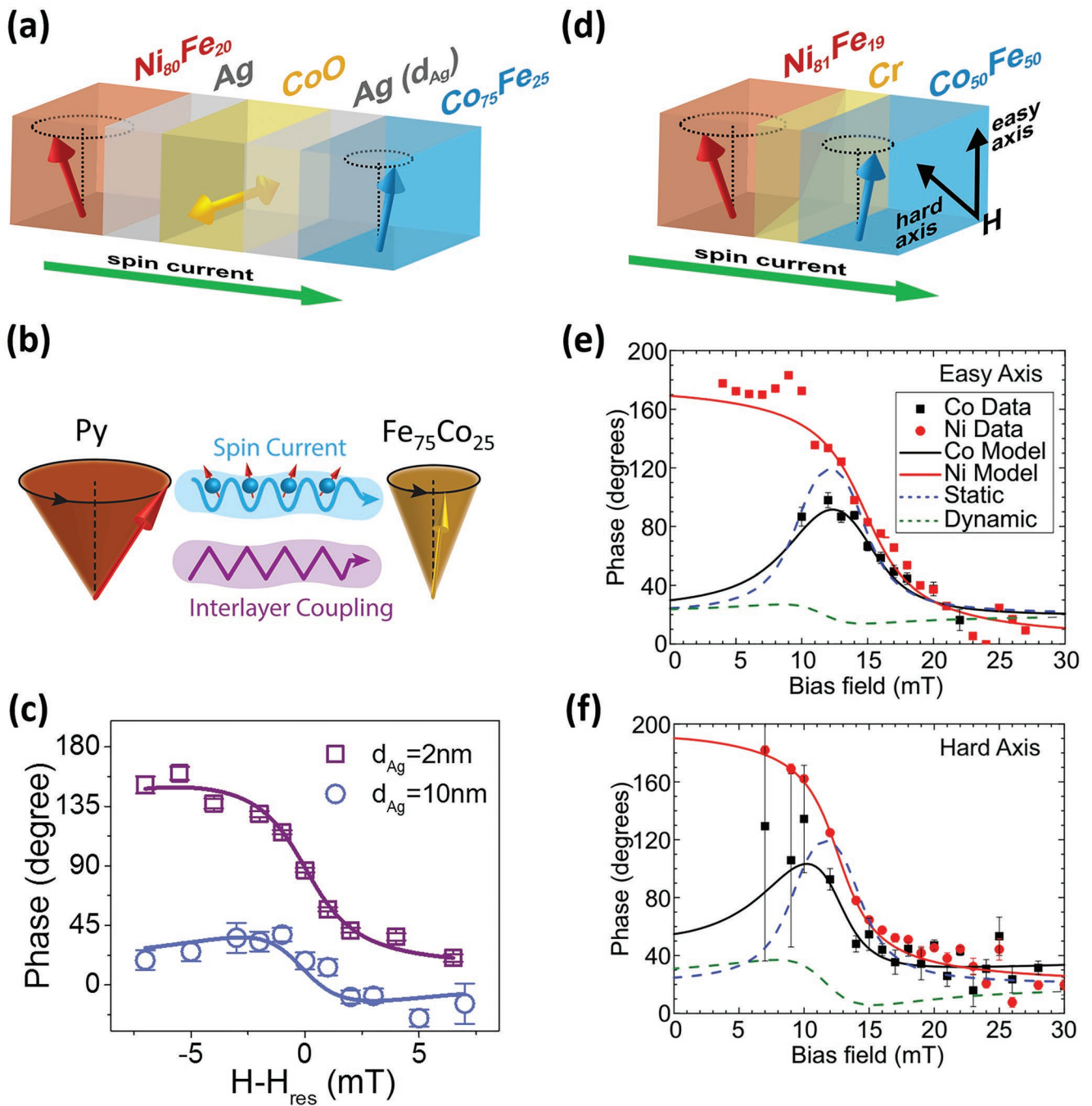
Figure 4: Study of interlayer coupling and spin current (dynamic coupling) in Py/Ag/CoO/Ag/Fe$_{75}$Co$_{25}$ (a–c), adapted from Q. Li et al. [28], and in Ni$_{81}$Fe$_{19}$/Cr/Fe$_{50}$Co$_{50}$ (d–f), adapted from Baker et al. [25]. (a, d) Schematic drawing of the sample structures. (b) Illustration of AC spin current and interlayer coupling as the driving mechanisms of Fe$_{75}$Co$_{25}$ spin precession originating from the Py FMR. (c) Phase of the Fe$_{75}$Co$_{25}$ spin precession in proximity to the FMR condition of Py within the multilayer sample with d$_{Ag}$= 2 and 10 nm. Phase of the Fe$_{50}$Co$_{50}$ spin precession in proximity to the FMR condition of Py with field applied along the (e) Fe$_{50}$Co$_{50}$ easy axis and the (f) Fe$_{50}$Co$_{50}$ hard axis direction.
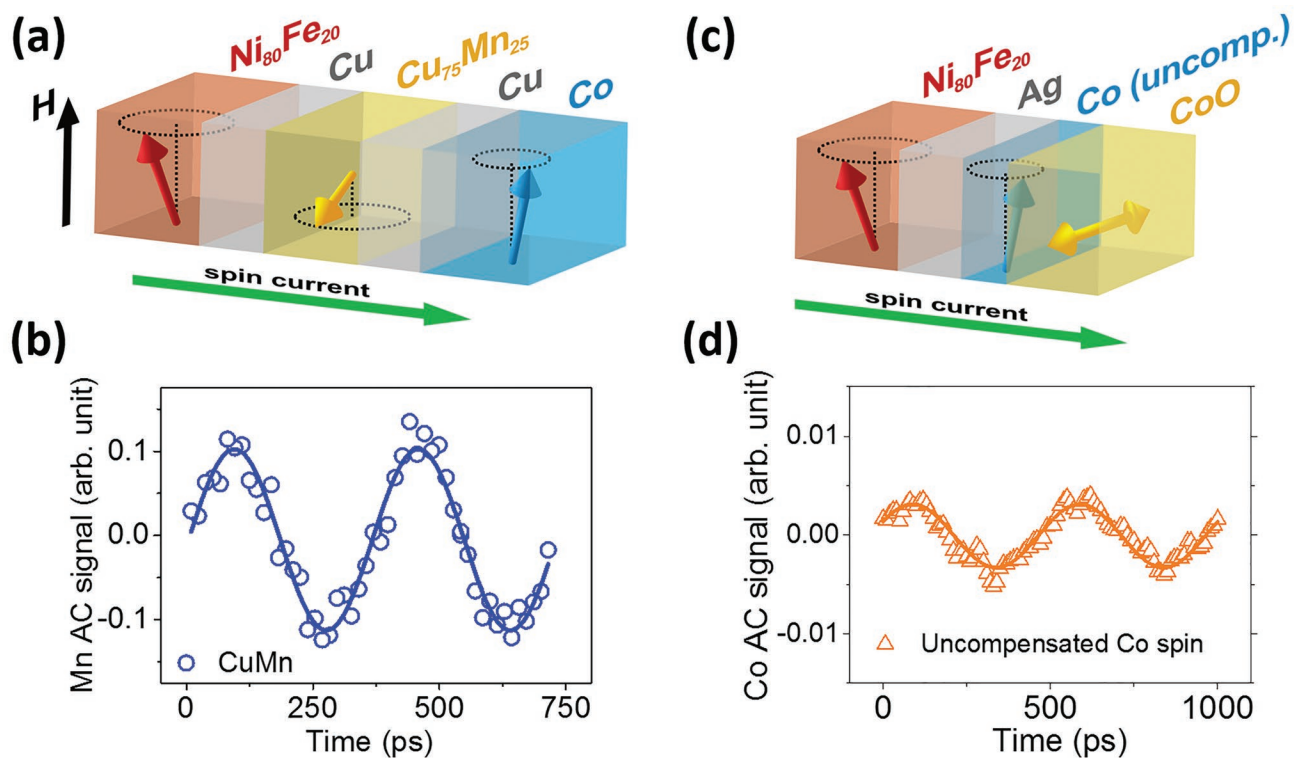
Figure 5: Schematic drawing of (a) the spin precession of paramagnetic $Cu_{75}Mn_{25}$ in $NiFe/Cu/Cu_{75}Mn_{25}/Cu/Co$ due to a spin current pumped by the Py FMR; and (c) the spin precession of uncompensated Co spins at the CoO interface in a Py/Ag/CoO heterostructure. The spin precession signal of $Cu_{75}Mn_{25}$ is shown in (b), and the Co ac signal is shown in (d). (a–b) is adapted from J. Li et al. [26], and (c–d) is adapted from Q. Li et al. [28].

at the interface of a CoO layer. Using XFMR, Q. Li et al. [28] were able to measure the magnetic excitation of uncompensated Co spins at the interface between Ag and CoO in a Py/Ag/CoO heterostructure (Figure 5(c)). The uncompensated FM Co spins precess near the Py FMR field, indicating a coupling between the Co moments and the Py source. The AC XMCD signal is three orders of magnitude smaller than the Py AC signal, but is still clearly observable, highlighting the high sensitivity of the XFMR technique.

Outlook

Lately, most studies utilizing XFMR have concentrated on the investigation of spin current transport in heterostructures as shown in Figure 3(a), with a focus on different interlayer materials [21, 26–30, 39]. AFM insulators in particular have received a great deal of interest, due to their interesting properties and their potential for use in spintronic applications. While XFMR using circularly polarized X-rays is a powerful tool to investigate spin currents propagating between the ferromagnetic spin source and spin sink layer, and can even probe spin-current-driven magnetic excitations in paramagnetic materials, the

direct observation of GHz spin current propagation within AFM insulators is not accessible. However, utilizing linearly polarized X-rays within XFMR experiments is a promising approach for the investigation of GHz excitations within AFMs. Similar to static X-ray magnetic linear dichroism (XMLD), this technique is sensitive to the spin axis rather than the spin direction and can provide magnetic contrast, even in the absence of a net magnetization. Therefore, it can help to provide detailed insight into the dynamic mechanisms that occur within AFM materials. This technique is currently being developed at beamline 4.0.2 of the ALS and has already been applied to different reference systems [28, 40].

XFMR was developed to study element-selective magnetization dynamics, thus giving layer resolution of the magneto-dynamics in technologically relevant multilayer samples. Note, however, that XFMR does not provide lateral resolution, so the modal structure of the dynamic magnetic modes remains unexplored. A major breakthrough was recently reported by Burn et al. [41] at Diamond Light Source by demonstrating the utilization of a novel diffractive ferromagnetic resonance (DFMR) technique for retrieving the phase-resolved dynamics of

References

1. A. J. Berger et al., *Phys. Rev. B* **97**, 094407 (2018).
2. W. E. Bailey et al., *Phys. Rev. B* **70**, 172403 (2004).
3. G. Boero et al., *Appl. Phys. Lett.* **87**, 152503 (2005).
4. J. Goulon et al., *JETP Lett.*, **82**, 696–701 (2005).
5. A. Puzic et al., *J. Appl. Phys.* **97**, 10E704 (2005).
6. D. A. Arena et al., *Phys. Rev. B* **74**, 064409 (2006).
7. J. Goulon et al., *Eur. Phys. J. B* **53**, 169–184 (2006).
8. Y. Guan et al., *J. Appl. Phys.* **99**, 08J305 (2006).
9. D. A. Arena et al., *J. Appl. Phys.* **101**, 09C109 (2007).
10. J. Goulon et al., *J. Electron Spectrosc.* **156–158**, 38–44 (2007).
11. J. Goulon et al., *J. Synchrotron Rad.* **14**, 257–271 (2007).
12. G. Boero et al., *New J. Phys.* **10**, 013011 (2008).
13. T. Martin et al., *J. Appl. Phys.* **103**, 07B112 (2008).
14. D. A. Arena et al., *Rev. Sci. Inst.* **80**, 083903 (2009).
15. G. Boero et al., *Phys. Rev. B* **79**, 224425 (2009).
16. G. Boero et al., *Rev. Sci. Inst.* **80**, 123902 (2009).
17. T. Martin et al., *J. Appl. Phys.* **105**, 07D310 (2009).
18. M. K. Marcham et al., *J. Appl. Phys.* **109**, 07D353 (2011).
19. W. E. Bailey et al., *Nat. Commun.* **4**, 2025 (2013).
20. M. K. Marcham et al., *Appl. Phys. Lett.* **102**, 062418 (2013).
21. A. A. Baker et al., *Sci. Rep.* **5**, 7907 (2015).
22. A. I. Figueroa et al., *J. Magn. Magn. Mater.* **400**, 178–183 (2016).
23. K. Ollefs et al., *J. Appl. Phys.* **117**, 223906 (2015).
24. T. Devolder, *J. Appl. Phys.* **119**, 153905 (2016).
25. A. A. Baker et al., *Phys. Rev. Lett.* **116**, 047201 (2016).
26. J. Li et al., *Phys. Rev. Lett.* **117**, 076602 (2016).
27. C. J. Durrant et al., *Phys. Rev. B* **96**, 144421 (2017).
28. Q. Li et al., *Nat. Commun.* **10**, 5265 (2019).
29. M. K. Marcham et al., *Phys. Rev. B* **87**, 180403(R) (2013).
30. A. A. Baker et al., *Sci. Rep.* **6**, 35582 (2016).
31. G. B. G. Stenning et al., *New J. Phys.* **17**, 013019 (2015).
32. A. A. Baker et al., *J. Magn. Magn. Mater.* **473**, 470–476 (2019).
33. G. van der Laan and A. I. Figueroa, *Coord. Chem. Rev.* **277–278**, 95–129 (2014).
34. G. van der Laan, *J. Electron Spectrosc. Relat. Phenom.* **220**, 137–146 (2017).
35. J. C. Slonczewski, *J. Mag. Mag. Mater.* **159**, L1–L7 (1996).
36. L. Berger, *Phys. Rev. B* **54**, 9353 (1996).
37. P. K. Manna, and S. M. Yusuf, *Phys. Rep.* **535**, 61–99 (2014).
38. Y. Meng et al., *Phys. Rev. B* **85**, 014425 (2014).
39. M. Dabrowski et al., arXiv:1912.05621 (2019).
40. C. Klewe et al., in preparation.
41. D. M. Burn et al., *Nano Lett.* **20**, 345−352 (2020).

individual spin modes at GHz frequencies and with nanoscale sensitivity in periodically structured spin systems. DFMR is built on two synchrotron-radiation based techniques: resonant elastic X-ray scattering and XFMR. The ability of this method to study distinct magnetic phases was demonstrated through measurements on Y-type hexaferrite, which contains a rich level of complexity. The use of this technique applied to further magnetic systems will allow complex magnetic dynamic processes to be investigated in the future.

Funding